Mechanics and Computational Homogenization of Effective Material Properties of Functionally Graded (Composite) Material Plate FGM

Christian Mathew [a], Oluomachi Ejiofor [b]

[a] Department of Engineering Mechanics, [b] Department of Computer Science
[a]Virginia Polytechnic Institute and State University, Blacksburg, 24061
[b]Austin Peay State University, Clarksville, Tennessee, 37044

DOI: 10.29322/IJSRP.13.09.2023.p14120
https://dx.doi.org/10.29322/IJSRP.13.09.2023.p14120

Paper Received Date: 2nd August 2023
Paper Acceptance Date: 4th September 2023
Paper Publication Date: 16th September 2023

Abstract- Functionally graded materials (FGMs) are categorized as functional composites, where the volume fractions of two or more materials change continuously based on position along specific dimensions (mainly through-the -thickness) of the structure to achieve desired functionality. A typical example of FGM is an inhomogeneous composite consisting of distinct phases of material constituents (e.g., ceramics and metals for thermal barrier structures), featuring a strong bending-stretching coupling effect. The overall properties of FGMs are unique and distinguishable from the individual materials comprising them. Mechanical properties exhibit continuous variation across the plate's thickness. Variations in constituent volume fractions lead to diverse microstructures. The effective properties of FGM plates are assumed to change along the thickness direction, following power law, sigmoid, and exponential distributions. FGMs are created by altering chemical composition, microstructure, or design features from one end to the other as required. They exhibit high-temperature resistance, efficiently mitigating thermal stresses and moisture impacts. The variation in volume fraction throughout the thickness is computed using different homogenization techniques, namely the rule of mixtures, Mori-Tanaka scheme, and self-consistent method. Several micromechanical models have been developed and utilized to estimate effective properties of these materials in relation to volume fraction distributions. The manipulated variable concerns the concentration of reinforcing particles at various points within the component. This study delves into various methods and theories for modeling and analyzing functionally graded materials, offering a comprehensive exploration of their features. The outcomes and new findings of this analysis are presented.

Index Terms- Effective material properties, FGM, homogenization, Volume fractions, Mori–Tanaka scheme, Rule of mixtures, Power law, Sigmoid law.

I. INTRODUCTION

In recent years, the demand for improved structural efficiency in aerospace engineering applications has led to the emergence of a new class of materials known as functionally graded materials (FGMs). FGMs are designed in a manner where material properties vary smoothly and continuously through-the-thickness, transitioning from the surface of a ceramic exposed to high temperatures to that of a metal on the opposite surface. They have been developed for general use as structural components in high-temperature environments. The composition of FGMs involves two distinct materials: an engineering ceramic, which resists thermal loading from the high-temperature environment, and a lightweight metal that maintains structural toughness. The primary objective of FGM development is to create materials capable of withstanding extreme temperatures, allowing ceramics to function as refractories (materials with excellent heat resistance) when combined with other substances. However, ceramics alone cannot be employed for engineering structures subjected to substantial mechanical loads due to their poor toughness properties. To address this limitation, ceramics need to be combined with materials possessing good toughness properties, such as metals and polymers, in order to leverage the advantages of each material. Composite materials are extensively employed in engineering applications due to their inherent mechanical properties, including high strength, modulus of elasticity, and lower specific gravity. The advancement of new composite materials with enhanced physical and mechanical properties has become achievable through extensive studies and research on the metallurgical aspects of materials, coupled with a better understanding of structural properties. One such material with the potential to meet specific requirements in various engineering applications and harness the benefits of individual material properties is the functionally graded material (FGM). This potential is rooted in the changing material composition of FGMs, which follows a defined law in a preferred direction.

FGMs find application in the design of aerospace structures, heat engine components, and nuclear power plants. Numerous research papers have been published to assess the behavior of FGMs using both experimental and numerical techniques, encompassing linearity

and nonlinearity across various domains. FGMs can be produced by gradually and continuously adjusting the constituents of multiphase materials according to a predetermined profile. The power law function, sigmoid function, and exponential function are commonly used by researchers to describe effective material properties.

Delale and Erdogan [1] indicated that the effect of Poisson's ratio on deformation is much less compared to that of Young's modulus. The primary concern in the mechanics of FGM materials is predicting the material's behavior. This requires estimating the effective (overall) properties of the composition throughout the thickness, a concept commonly known as homogenization. The effective elastic moduli of the graded microstructures must be evaluated using the volume fraction distribution and the approximate shape of the dispersed phase when precise information about the size, shape, and distribution of phases is not available. Over the years, several micromechanical models have been developed to describe the effective properties of both macroscopically homogeneous composites and functionally graded materials [2-5]. The rule of mixtures, also known as the Voigt model [6-9], is the most popular and widely used model to estimate through-the-thickness properties of FGMs. Mori–Tanaka homogenization scheme [10-14], and self-consistent schemes [9, 15-17] were reported in the literature and used to determine the bounds for the effective properties of FGM. Comparisons have been made with reference to the self-consistent scheme. However, there is a scarcity of comparison between the results obtained from these models with analytical solutions or experimental results. Results obtained from the open literature indicate that the Voigt and Mori–Tanaka schemes have been adopted for studying FGM structures by most researchers [18-20]. Reddy and Cheng [21] have considered the variation of material properties through the thickness according to a power-law distribution, and the locally effective material properties obtained in terms of the volume fractions of the constituents by the Mori–Tanaka scheme. These works focus on the parametric effects of the power-law index or other parameters of the models on the response of FGM composite. Moreover, it has been observed that while many researchers use the rule of mixtures with a power-law approach for material homogenization, only a few have attempted a comparison of the rule of mixture with the Mori–Tanaka scheme.

The goal of this study is to understand the influence of a homogenization scheme (effective material properties through the thickness) and to identify simple models that provide accurate estimates of effective properties over the entire range of volume fractions with minimal or no empirical fitting parameters and minimal computational effort. Three homogenization schemes, namely the rule of mixtures, the Mori–Tanaka scheme, and the self-consistent scheme, have been used to estimate the effective properties. The material properties of the plate are considered to vary according to a power-law distribution across the thickness of the plate.

Problem description

An elastic rectangular plate is considered, characterized by coordinates $x, y,$ and z. The xy plane defines the plate's plane, while the z-axis represents its thickness direction. The material properties, including Young's modulus and Poisson's ratio, are known on both the upper and lower surfaces, tailored to the design requirements. These material properties, such as Young's modulus and Poisson's ratio, exhibit continuous variation along the thickness direction (z-axis), denoted as $E = E(z)$ and $v = v(z)$ respectively. This type of material configuration is referred to as a functionally graded material.

As shown in Figure 1, the composite structure comprises metal the bottom surface to impart toughness and ceramics at the top surface to provide refractoriness, each serving specific purposes within the design.

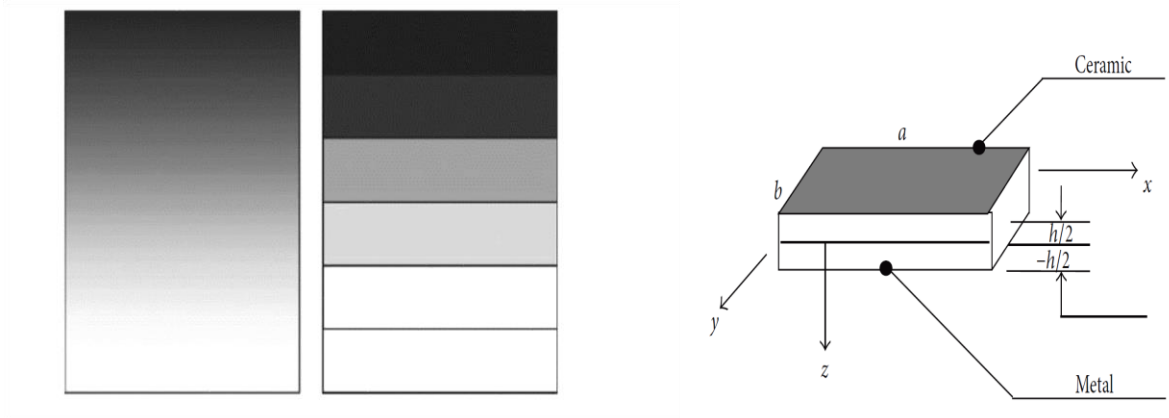

Fig 1: Description of functionally graded plate FGM [22].

Power law distribution

In a two-constituent metal-ceramic functionally graded material (FGM) layer, where the volume fractions of the constituent phases are distributed throughout the layer thickness, a prescribed distribution can be established using a typical power-law function. For an FGM layer that is rich in ceramics on its upper surface, the volume fraction $Vc(z)$ of the functional graded material follows power-law functions as defined below.

$$V_c(z) = V_c^b + (V_c^t - V_c^b)\left(\frac{1}{2} + \frac{z}{h}\right)^n \qquad 1a$$

For a FGM layer ceramic-rich on its bottom surface, the volume fraction $V_c(z)$ of functional graded material is given by

$$V_c(z) = V_c^t + (V_c^b - V_c^t)\left(\frac{1}{2} + \frac{z}{h}\right)^n \quad 2b$$

where V_c^t and V_c^b are the volume fractions of the ceramic phase on the top and bottom surfaces of the FGM laminae respectively, and n is a scalar parameter or power law index that dictates the material gradation profile through the layer thickness. The most commonly used FGM layer metal-ceramic FGM with ceramic-rich on its top surface with $V_c^t = 1$ and $V_c^b = 0$, and metal rich on its bottom surface with $V_m^t = 0$ and $V_m^b = 1$.

Hence the volume fraction of the metal phase $V_m(z)$ and ceramic phase are subsequently defined since $V_c(z) + V_m(z) = 1$, in other words $0 \leq Vc(z) \leq 1$ and $0 \leq Vm(z) \leq 1$.

Sigmoid law distribution

Due to the continuous change in the volume fraction of the constituent materials within the Functionally Graded Material (FGM), the material properties vary continuously through the thickness direction according to a sigmoid function. In the case of a single power-law function, stress concentrations appear at one of the interfaces where the material is continuous but changes rapidly across the interface. To address this, the volume fraction is calculated using two power-law functions, ensuring that the material properties are smoothly distributed across the interfaces.

$$V_c(z) = \frac{1}{2}\left(1 + \frac{2z}{h}\right)^n \qquad 0 \leq z \leq \frac{h}{2} \quad 2a$$

$$V_c(z) = 1 - \frac{1}{2}\left(1 - \frac{2z}{h}\right)^n \qquad -\frac{1}{2} \leq z \leq 0 \quad 2b$$

Exponential Law

The mechanical material properties vary continuously throughout the thickness direction exponentially, in accordance with the volume fraction of constituents. This function is more convenient than a power law because it lacks a power index, and the properties of the Functionally Graded Material (FGM) depend solely on ceramic and material properties. It directly generates the Young's modulus and other material properties across the thickness without the need to calculate the volume fraction first. This approach is most suitable for fracture mechanics problems.

$$E(z) = E_t\left(\exp\left(\frac{1}{h} ln \frac{E_b}{E_t}\right)\left(z + \frac{h}{2}\right)\right) \quad 3a$$

$$v(z) = v_t\left(\exp\left(\frac{1}{h} ln \frac{v_b}{v_t}\right)\left(z + \frac{h}{2}\right)\right) \quad 3b$$

where h is the non-dimensional thickness of the plate and z is a point through the thickness.

Homogenization techniques

Homogenization techniques encompass various methods used to estimate the effective properties at a given point in a material. These techniques include the rule of mixture, Mori–Tanaka method, self-consistent method, and more. These methods are commonly applied to estimate the effective material properties of functionally graded composites.

Rule of mixture

The rule of mixture, often associated with the Voigt model, involves estimating the effective properties of a composite material, such as a metal-ceramic functionally graded material (FGM) composed of aluminum and silicon carbide. This estimation is achieved by calculating a weighted average based on the volume fractions of the respective constituents' properties. The properties derived from this model serve as both the upper and lower bounds for the effective elastic properties of the heterogeneous material.

$$P(z) = \sum_i^k P_i V_{c(i)}(z)$$

$$P(z) = (P_t - P_b)V_c(z) + P_b \quad 4$$

where $P(z)$ is any material property through the thickness z, P_t and P_t are the properties at top and bottom surface of the plate respectively, k is the number of the material phase to be homogenized.

The mechanical material properties of a FGM can be determined by the rule of mixture as shown below

$$E(z) = (E_t - E_b)V_c(z) + E_b \quad 5a$$

$$v(z) = (v_t - v_b)V_c(z) + v_b \quad 5b$$

Hence, $E(z)$ is the effective modulus of elasticity, $v(z)$ is Poisson's ratio, each varying through the thickness. For a given isotropic material, bulk modulus and shear modulus are estimate as shown below in eq. (6)

$$B(z) = \frac{E(z)}{3(1-2v(z)} \quad 6a$$

$$G(z) = \frac{E(z)}{2(1+2v(z)} \quad 6b$$

where $B(z)$ is the bulk modulus $G(z)$ is the shear modulus.

When hygro-thermo-mechanical properties are considered, the following additional quantities are incorporated as shown in eq. (7)

$$\alpha(z) = (\alpha_t - \alpha_b)V_c(z) + \alpha_b$$

$$\beta(z) = (\beta_t - \alpha_b)V_c(z) + \beta_b \qquad k(z) = (k_t - k_b)V_c(z) + k_b \qquad D(z) = (D_t - D_b)V_c(z) + D_b \qquad 7$$

where $\alpha(z)$ are coefficients of thermal expansion, $k(z)$ are coefficients of thermal conductivity coefficient, $\beta(z)$ are coefficients of moisture expansion, and $D(z)$ are the coefficients of mass diffusivity

when density and yield strength are considered, eq. (8) hold

$$\rho(z) = (\rho_t - \rho_b)V_c(z) + \rho_b \qquad 8a$$

$$\sigma_y(z) = \left(\sigma_{yt} - \sigma_{yb}\right)V_c(z) + \sigma_{yb} \qquad 8b$$

where $\rho(z)$ is the dry mass density, and $\sigma_y(z)$ is the ultimate yield strength. The subscript b denotes the bottom surface i.e., the metal phase, and the subscript t denotes the top surface i.e., the ceramic phase.

Mori-Tanaka technique

The Mori-Tanaka method [12, 23] is particularly suitable for a graded composite microstructure that possesses a well-defined, continuous, isotropic matrix phase. This matrix phase is reinforced by a random distribution of isotropic particles from a particulate phase. The following equations are used to estimate the effective material properties of a functionally graded material using the aforementioned technique.

$$\frac{B(z)-B_1}{B_2-B_1} = \frac{V_2(z)}{1+(1-V_2(z)\frac{B_2-B_1}{B_1+\frac{4}{3}G_1}} \qquad 9a$$

$$\frac{G(z)-G_1}{G_2-G_1} = \frac{V_2(z)}{1+(1-V_2(z)\frac{G_2-G_1}{G_1+f_1}} \qquad 9b$$

$$\frac{\alpha(z)-\alpha_1}{\alpha_2-\alpha_1} = \frac{\frac{1}{B(z)}-\frac{1}{B_1}}{\frac{1}{B_2}-\frac{1}{B_1}} \qquad 10b$$

$$\frac{k(z)-k_1}{k_2-k_1} = \frac{V_2(z)}{1+(1-V_2(z)\frac{k_2-k_1}{3k_1}} \qquad 10b$$

$$\frac{\beta(z)-\beta_1}{\beta_2-\beta_1} = \frac{\frac{1}{B(z)}-\frac{1}{B_1}}{\frac{1}{B_2}-\frac{1}{B_1}} \qquad 11a$$

$$\frac{D(z)-D_1}{D_2-D_1} = \frac{V_2(z)}{1+(1-V_2(z)\frac{D_2-D_1}{3D_1}} \qquad 11b$$

$$E(z) = \frac{9B(z)G(z)}{3B(z)+G(z)} \qquad 12a$$

$$v(z) = \frac{3B(z)-2G(z)}{2(3B(z)+G(z))} \qquad 12b$$

where $f_1 = \frac{G_1(9B_t-8G_t)}{6(B_t-2G_t)}$, $E(z)$ is the effective Young's modulus, $v(z)$ is Poisson's ratio, $B(z)$ is the bulk modulus, $G(z)$ is the shear modulus, $\alpha(z)$ is thermal expansion coefficient, $k(z)$ is thermal conductivity coefficient, $D(z)$ is the mass diffusivity coefficients, $\beta(z)$ moisture expansion coefficients. Subscript 1 denotes the matrix phase (metal), and subscript 2 denotes the particulate phase (ceramics). In the numerical results, the metal is taken as the matrix phase and the ceramic is taken as the particulate phase. The volume fraction of the ceramic phase is given by

$$V_2(z) = V_c(z) = V_c^t + (V_c^b - V_c^t)\left(\frac{1}{2} + \frac{z}{h}\right)^n \qquad 13$$

where t (ceramic), and b (metal) correspond to 2 and 1 respectively.

Self-consistent estimate

The Self-Consistent estimate homogenization scheme was initially developed to estimate the equivalent stiffness of polycrystals while considering the interaction between the matrix and the grains, following Eshelby's formulation. This approach is based on the concept that the presence of a single inhomogeneity does not significantly alter the effective material properties within a system containing numerous inclusions [24]. Self-Consistent models are often referred to as embedding models, as they assume that each reinforcing inclusion is embedded within a continuous material, with the composite's effective properties being those of this continuum. This method does not differentiate between the matrix and reinforcement phases, resulting in the prediction of the same overall moduli in another composite where the roles of the phases are switched. As a result, this approach is particularly useful for determining the effective moduli in regions characterized by an interconnected skeletal microstructure. The implicit expressions for bulk modulus and shear modulus are provided below.

$$B(z) = \left(\frac{V_1}{(B_1+\frac{4G(z)}{3})} + \frac{V_2}{(B_2+\frac{4G(z)}{3})} - \frac{4G(z)}{3}\right)^{-1} \qquad 14a$$

$$\frac{V_1B_1}{(B_1+\frac{4G(z)}{3})} + \frac{V_2B_2}{(B_2+\frac{4G(z)}{3})} = -5\left(\frac{V_1G_2}{G(z)-G_2} + \frac{V_2G_1}{G(z)-G_1}\right) - 2 \qquad 14b$$

The self-consistent estimate of the thermal coefficients conductivity in the implicit form

$$\frac{V_1(B_1-k(z)}{k_1+2k(z)}+\frac{V_2(B_2-k(z)}{k_2+2k(z)}=0 \qquad 15a$$

$$\frac{\alpha(z)-\alpha_1}{\alpha_2-\alpha_1}=\frac{\frac{1}{B(z)}-\frac{1}{B_1}}{\frac{1}{B_2}-\frac{1}{B_1}} \qquad 15b$$

Due to the rigorous process involve in solving the quadratic equations in eq. (14a) and eq. (14b), it is easier to use the rule of mixture and Mori-Tanaka technique than Self-consistent method to estimate the effective material properties of functionally graded composite.

Other techniques use to analyze the effective material properties of functionally graded material are given in details in [25], are composite sphere assemblage model, composite cylindrical assemblage model, the simplified strength of materials method, the method of cells, micromechanical models, mathematical idealization of FGMs.

Numerical results and discussion

The following tables and plot show the through-thickness variation of the volume fraction of the metal-ceramic and Monel-zirconia FGM for power indices n=0.4, 0.8, 1,2, 1.8, 2.8, and 6. The material properties used for our analysis are shown.

Table 1: Mechanical and thermal properties of the materials used have the following values [26].

Material property		Aluminum	Silicon Carbide	Monel	Zirconia
E_{11}	GPa	70	427.0	179.4	151.0
$E_{22}=E_{33}$	GPa	70	427.0	179.4	151.0
$G_{12}=G_{13}$	GPa	26.923	182.479	65.55	58.077
G_{23}	GPa	26.923	182.479	65.55	58.077
$v_{12}=v_{13}=v_{23}$	----	0.3	0.17	0.3684	0.30
α_1	$10^{-6}/K$	23.4	4.3	15	10
$\alpha_2=\alpha_3$	$10^{-6}/K$	23.4	4.3	15	10
k_{11}	$W/(mK)$	233	65	25	2.09
$k_{22}=k_{22}$	$W/(mK)$	233	65	25	2.09
β_1	$10^{-4}/(Kg/m^3)$	4.0 1.481	0.01 0.003	4.0 0.455	0.01 0.002
$\beta_2=\beta_3$	$10^{-4}/(Kg/m^3)$	4.0 1.481	0.01 0.003	4.0 0.455	0.01 0.002
D_{11}	$10^{-12}(m^2)/s)$	0.02	0.2	0.02	0.02
$D_{22}=D_{33}$	$10^{-12}(m^2)/s$	0.02	0.2	0.02	0.02
p_{dry}	kg/m^3	2700	3210	8800	5700

Case 1; Rule of mixture

The results of the effective material properties of case 1 computed using the power law index distribution are presented. Table 1.1-1.4 and fig 1.1-1.4 describe the variation of effective material properties through-the-thickness.

Table 1.1: Power law index n and corresponding volume fraction through-the-thickness.

z/h	n=0.4	0.8	1.2	1.8	2.8	6
0.0150	1	1	1	1	1	1
0.0125	0.9658	0.9328	0.9009	0.8550	0.7838	0.5933
0.0100	0.9297	0.8643	0.8035	0.7202	0.6002	0.3349
0.0075	0.8913	0.7944	0.7081	0.5958	0.4469	0.1780
0.0050	0.8503	0.7230	0.6147	0.4820	0.3213	0.0878

0.0025	0.8061	0.6497	0.5237	0.3790	0.2211	0.0394
0	0.7579	0.5743	0.4353	0.2872	0.1436	0.0156
-0.0025	0.7046	0.4964	0.3497	0.2068	0.0862	0.0052
-0.0050	0.6444	0.4152	0.2676	0.1384	0.0461	0.0014
-0.0075	0.5743	0.3299	0.1895	0.0825	0.0206	2.4414e-04
-0.0100	0.4884	0.2385	0.1165	0.0397	0.0066	2.1433e-05
-0.0125	0.3701	0.1370	0.0507	0.0114	9.5125e-04	3.3490e-07
-0.0150	0	0	0	0	0	0

Table 1.2: Power law index n and corresponding elasticity modulus through-the-thickness.

z/h	**n=0.4**	**0.8**	**1.2**	**1.8**	**2.8**	**6**
0.0150	4.2700e+11	4.2700e+11	4.2700e+11	4.2700e+11	4.2700e+11	4.2700e+11
0.0125	4.1479e+11	4.0299e+11	3.9160e+11	3.7525e+11	3.4981e+11	2.8181e+11
0.0100	4.0189e+11	3.7855e+11	3.5685e+11	3.2712e+11	2.8427e+11	1.8956e+11
0.0075	3.8819e+11	3.5361e+11	3.2278e+11	2.8271e+11	2.2953e+11	1.3354e+11
0.0050	3.7355e+11	3.2810e+11	2.8946e+11	2.4207e+11	1.8471e+11	1.0134e+11
0.0025	3.5776e+11	3.0195e+11	2.5697e+11	2.0531e+11	1.4893e+11	8.4066e+10
0	3.4056e+11	2.7504e+11	2.2539e+11	1.7252e+11	1.2126e+11	7.5578e+10
-0.0025	3.2153e+11	2.4721e+11	1.9486e+11	1.4384e+11	1.0077e+11	7.1868e+10
-0.0050	3.0005e+11	2.1824e+11	1.6553e+11	1.1941e+11	8.6471e+10	7.0490e+10
-0.0075	2.7504e+11	1.8777e+11	1.3764e+11	9.9442e+10	7.7360e+10	7.0087e+10
-0.0100	2.4434e+11	1.5514e+11	1.1158e+11	8.4190e+10	7.2365e+10	7.0008e+10
-0.0125	2.0213e+11	1.1890e+11	8.8099e+10	7.4075e+10	7.0340e+10	7.0000e+10
-0.0150	7.0000e+10	7.0000e+10	7.0000e+10	7.0000e+10	7.0000e+10	7.0000e+10

Table 1.3: Power law Index and corresponding Poisson's ratio through-the-thickness.

z/h	n=0.4	0.8	1.2	1.8	2.8	6
0.0150	0.1700	0.1700	0.1700	0.1700	0.1700	0.1700
0.0125	0.1744	0.1787	0.1829	0.1888	0.1981	0.2229
0.0100	0.1791	0.1876	0.1955	0.2064	0.2220	0.2565
0.0075	0.1841	0.1967	0.2080	0.2225	0.2419	0.2769
0.0050	0.1895	0.2060	0.2201	0.2373	0.2582	0.2886
0.0025	0.1952	0.2155	0.2319	0.2507	0.2713	0.2949
0	0.2015	0.2253	0.2434	0.2627	0.2813	0.2980
-0.0025	0.2084	0.2355	0.2545	0.2731	0.2888	0.2993
-0.0050	0.2162	0.2460	0.2652	0.2820	0.2940	0.2998
-0.0075	0.2253	0.2571	0.2754	0.2893	0.2973	0.3000
-0.0100	0.2365	0.2690	0.2849	0.2948	0.2991	0.3000
-0.0125	0.2519	0.2822	0.2934	0.2985	0.2999	0.3000
-0.0150	0.3000	0.3000	0.3000	0.3000	0.3000	0.3000

Table 1.4: Power law Index (n) and corresponding coefficient of thermal deformation through-the-thickness.

z/h	n=0.4	0.8	1.2	1.8	2.8	6
0.0150	4.3000e-06	4.3000e-06	4.3000e-06	4.3000e-06	4.3000e-06	4.3000e-06
0.0125	4.9533e-06	5.5843e-06	6.1937e-06	7.0690e-06	8.4299e-06	1.2068e-05
0.0100	5.6434e-06	6.8922e-06	8.0533e-06	9.6435e-06	1.1936e-05	1.7003e-05
0.0075	6.3761e-06	8.2266e-06	9.8759e-06	1.2020e-05	1.4865e-05	2.0001e-05
0.0050	7.1596e-06	9.5911e-06	1.1658e-05	1.4194e-05	1.7263e-05	2.1723e-05
0.0025	8.0043e-06	1.0990e-05	1.3397e-05	1.6161e-05	1.9177e-05	2.2647e-05
0	8.9249e-06	1.2430e-05	1.5086e-05	1.7915e-05	2.0657e-05	2.3102e-05

-0.0025	9.9430e-06	1.3919e-05	1.6720e-05	1.9449e-05	2.1754e-05	2.3300e-05
-0.0050	1.1092e-05	1.5469e-05	1.8289e-05	2.0756e-05	2.2519e-05	2.3374e-05
-0.0075	1.2430e-05	1.7099e-05	1.9781e-05	2.1825e-05	2.3006e-05	2.3395e-05
-0.0100	1.4072e-05	1.8845e-05	2.1175e-05	2.2641e-05	2.3273e-05	2.3400e-05
-0.0125	1.6331e-05	2.0784e-05	2.2432e-05	2.3182e-05	2.3382e-05	2.3400e-05
-0.0150	2.3400e-05	2.3400e-05	2.3400e-05	2.3400e-05	2.3400e-05	2.3400e-05

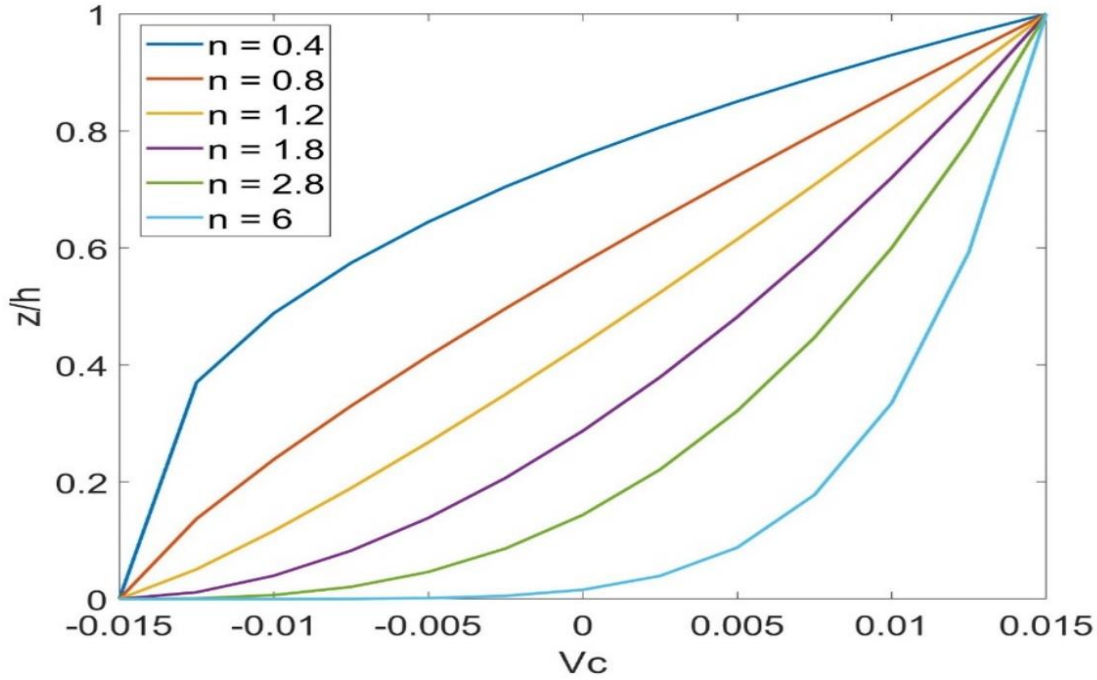

Fig 1.1: Through-the-thickness distribution of the volume fraction of the ceramic phase in the functionally graded plate.

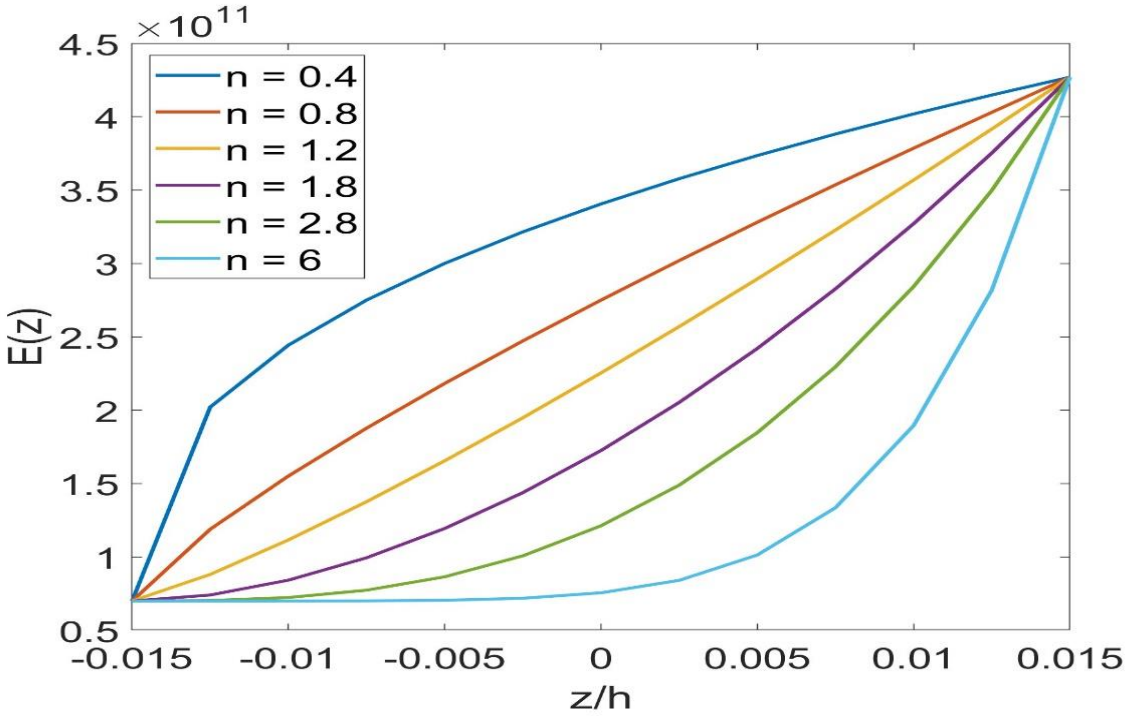

Fig 1.2: Variation of Young's modulus with the non-dimensional thickness for different values of power index n.

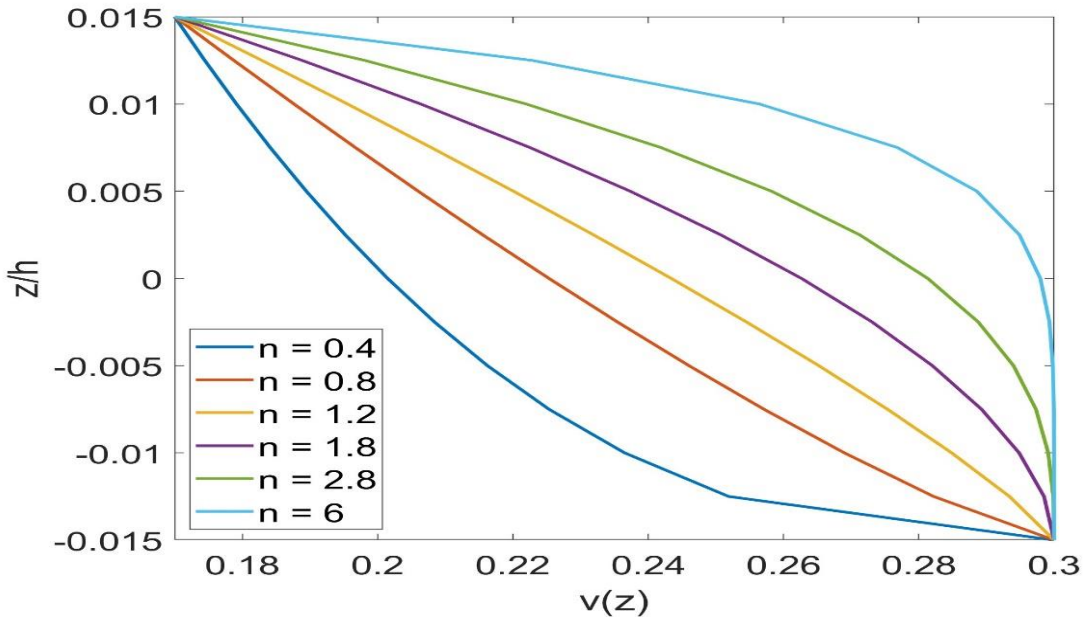

Fig 1.3: Variation of Poisson's ratio with the non-dimensional thickness for different values of power index n.

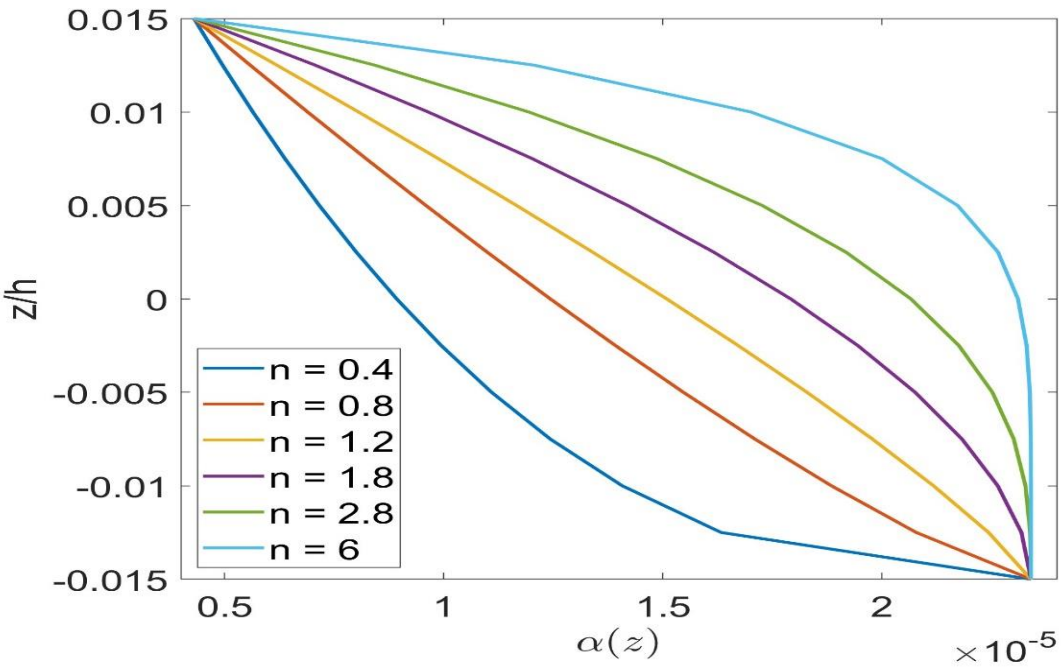

Fig 1.4: Variation of coefficient of thermal deformation with the non-dimensional thickness for different values of power index n.

Result of case 1 with Sigmoid law distribution

The results of the effective material properties of case 1 computed using the sigmoid law distribution are presented. Table 1.5-1.8 and fig 1.5-1.8 describe the smooth transfer of material properties across the interface unlike the ones obtained using one single power law index.

Table 1.5: Sigmoid Law Distribution index n and corresponding volume fraction through-the-thickness.

z/h	n=0.4	0.8	1.2	1.8	2.8	6
0.0150	1	1	1	1	1	1
0.0125	0.7558	0.8808	0.9418	0.9801	0.9967	1.0000
0.0100	0.6778	0.7924	0.8662	0.9308	0.9769	0.9993
0.0075	0.6211	0.7128	0.7824	0.8564	0.9282	0.9922
0.0050	0.5749	0.6385	0.6926	0.7590	0.8393	0.9561
0.0025	0.5352	0.5679	0.5983	0.6399	0.6999	0.8326
0	0.5000	0.5000	0.5000	0.5000	0.5000	0.5000
-0.0025	0.4648	0.4321	0.4017	0.3601	0.3001	0.1674
-0.0050	0.4251	0.3615	0.3074	0.2410	0.1607	0.0439
-0.0075	0.3789	0.2872	0.2176	0.1436	0.0718	0.0078

-0.0100	0.3222	0.2076	0.1338	0.0692	0.0231	6.8587e-04
-0.0125	0.2442	0.1192	0.0582	0.0199	0.0033	1.0717e-05
-0.0150	0	0	0	0	0	0

Table 1.6: Sigmoid Law Distribution index (n) and corresponding Young's modulus through-the-thickness.

z/h	**n=0.4**	**0.8**	**1.2**	**1.8**	**2.8**	**6**
0.0150	4.2700e+11	4.2700e+11	4.2700e+11	4.2700e+11	4.2700e+11	4.2700e+11
0.0125	3.3983e+11	3.8443e+11	4.0621e+11	4.1990e+11	4.2582e+11	4.2700e+11
0.0100	3.1198e+11	3.5288e+11	3.7924e+11	4.0229e+11	4.1876e+11	4.2676e+11
0.0075	2.9172e+11	3.2448e+11	3.4930e+11	3.7574e+11	4.0137e+11	4.2421e+11
0.0050	2.7522e+11	2.9795e+11	3.1727e+11	3.4097e+11	3.6964e+11	4.1133e+11
0.0025	2.6105e+11	2.7273e+11	2.8358e+11	2.9844e+11	3.1987e+11	3.6722e+11
0	2.4850e+11	2.4850e+11	2.4850e+11	2.4850e+11	2.4850e+11	2.4850e+11
-0.0025	2.3595e+11	2.2427e+11	2.1342e+11	1.9856e+11	1.7713e+11	1.2978e+11
-0.0050	2.2178e+11	1.9905e+11	1.7973e+11	1.5603e+11	1.2736e+11	8.5671e+10
-0.0075	2.0528e+11	1.7252e+11	1.4770e+11	1.2126e+11	9.5630e+10	7.2789e+10
-0.0100	1.8502e+11	1.4412e+11	1.1776e+11	9.4707e+10	7.8236e+10	7.0245e+10
-0.0125	1.5717e+11	1.1257e+11	9.0790e+10	7.7095e+10	7.1183e+10	7.0004e+10
-0.0150	7.0000e+10	7.0000e+10	7.0000e+10	7.0000e+10	7.0000e+10	7.0000e+10

Table 1.7: Sigmoid Law Distribution index (n) and corresponding Poisson's ratio through-the-thickness.

z/h	**n=0.4**	**0.8**	**1.2**	**1.8**	**2.8**	**6**
0.0150	0.1700	0.1700	0.1700	0.1700	0.1700	0.1700
0.0125	0.2017	0.1855	0.1776	0.1726	0.1704	0.1700
0.0100	0.2119	0.1970	0.1874	0.1790	0.1730	0.1701

0.0075	0.2193	0.2073	0.1983	0.1887	0.1793	0.1710
0.0050	0.2253	0.2170	0.2100	0.2013	0.1909	0.1757
0.0025	0.2304	0.2262	0.2222	0.2168	0.2090	0.1918
0	0.2350	0.2350	0.2350	0.2350	0.2350	0.2350
-0.0025	0.2396	0.2438	0.2478	0.2532	0.2610	0.2782
-0.0050	0.2447	0.2530	0.2600	0.2687	0.2791	0.2943
-0.0075	0.2507	0.2627	0.2717	0.2813	0.2907	0.2990
-0.0100	0.2581	0.2730	0.2826	0.2910	0.2970	0.2999
-0.0125	0.2683	0.2845	0.2924	0.2974	0.2996	0.3000
-0.0150	0.3000	0.3000	0.3000	0.3000	0.3000	0.3000

Table 1.8: Sigmoid Law Distribution index (n) and corresponding coefficients of thermal deformation through-the-thickness.

z/h	**n=0.4**	**0.8**	**1.2**	**1.8**	**2.8**	**6**
0.0150	4.3000e-06	4.3000e-06	4.3000e-06	4.3000e-06	4.3000e-06	4.3000e-06
0.0125	8.9638e-06	6.5776e-06	5.4123e-06	4.6796e-06	4.3633e-06	4.3002e-06
0.0100	1.0454e-05	8.2656e-06	6.8554e-06	5.6219e-06	4.7406e-06	4.3131e-06
0.0075	1.1538e-05	9.7850e-06	8.4569e-06	7.0425e-06	5.6713e-06	4.4492e-06
0.0050	1.2420e-05	1.1204e-05	1.0171e-05	8.9030e-06	7.3687e-06	5.1384e-06
0.0025	1.3178e-05	1.2554e-05	1.1973e-05	1.1178e-05	1.0032e-05	7.4983e-06
0	1.3850e-05	1.3850e-05	1.3850e-05	1.3850e-05	1.3850e-05	1.3850e-05
-0.0025	1.4522e-05	1.5146e-05	1.5727e-05	1.6522e-05	1.7668e-05	2.0202e-05
-0.0050	1.5280e-05	1.6496e-05	1.7529e-05	1.8797e-05	2.0331e-05	2.2562e-05
-0.0075	1.6162e-05	1.7915e-05	1.9243e-05	2.0657e-05	2.2029e-05	2.3251e-05
-0.0100	1.7246e-05	1.9434e-05	2.0845e-05	2.2078e-05	2.2959e-05	2.3387e-05
-0.0125	1.8736e-05	2.1122e-05	2.2288e-05	2.3020e-05	2.3337e-05	2.3400e-05

-0.0150	2.3400e-05	2.3400e-05	2.3400e-05	2.3400e-05	2.3400e-05	2.3400e-05

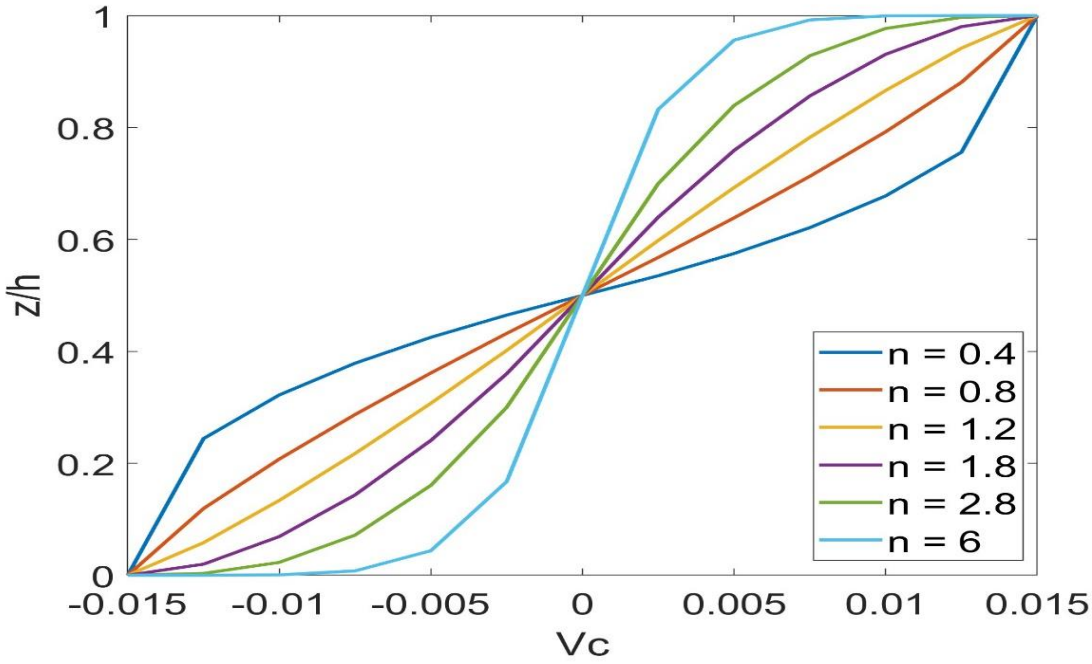

Fig 1.5: Through-the-thickness distribution of the volume fraction of the ceramic phase in the functionally graded plate.

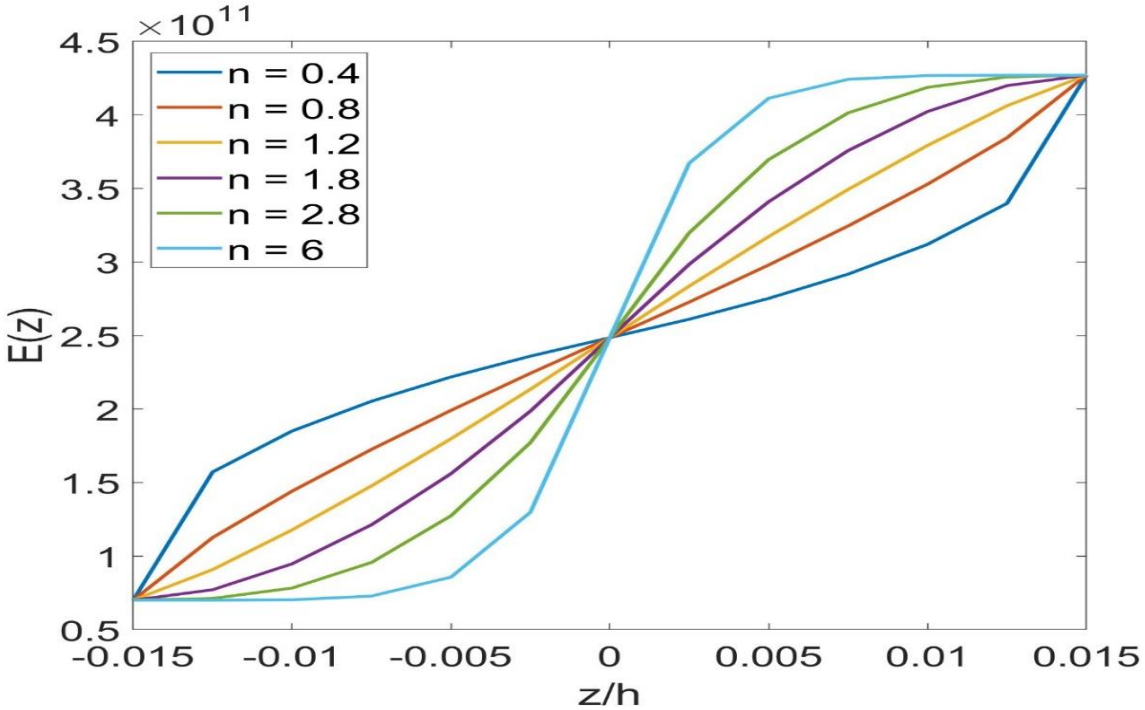

Fig 1.6: Variation of Young's modulus with the non-dimensional thickness for different values of Sigmoid law index n

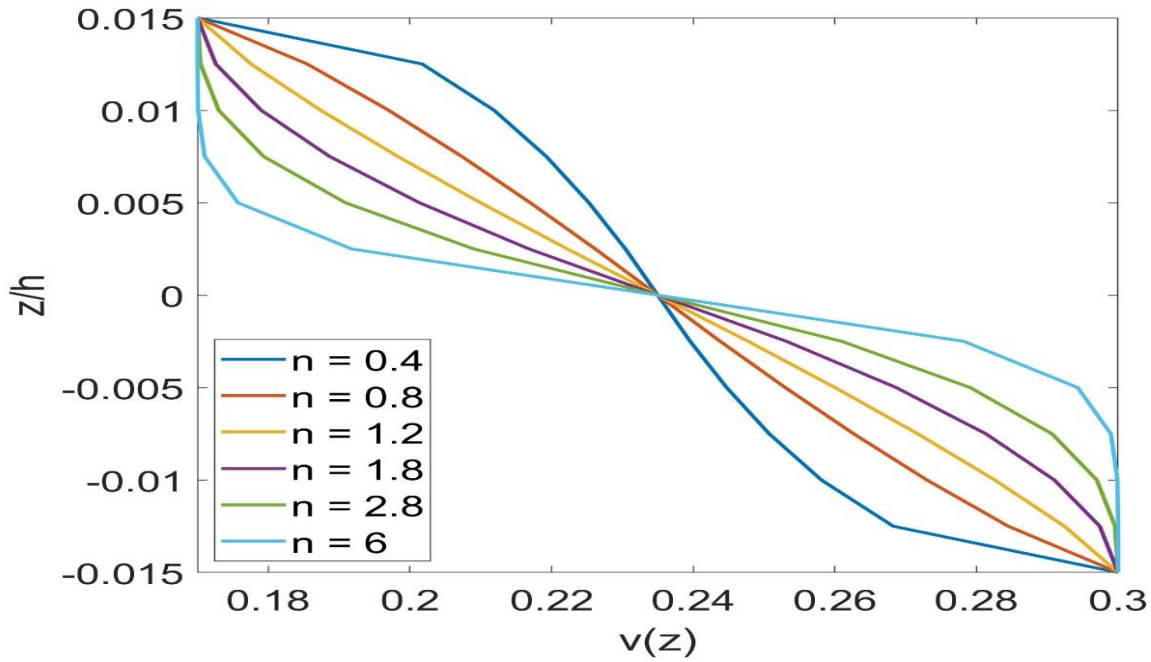

Fig 1.7: Variation of Poisson's ratio with the non-dimensional thickness for different values of Sigmoid law index n.

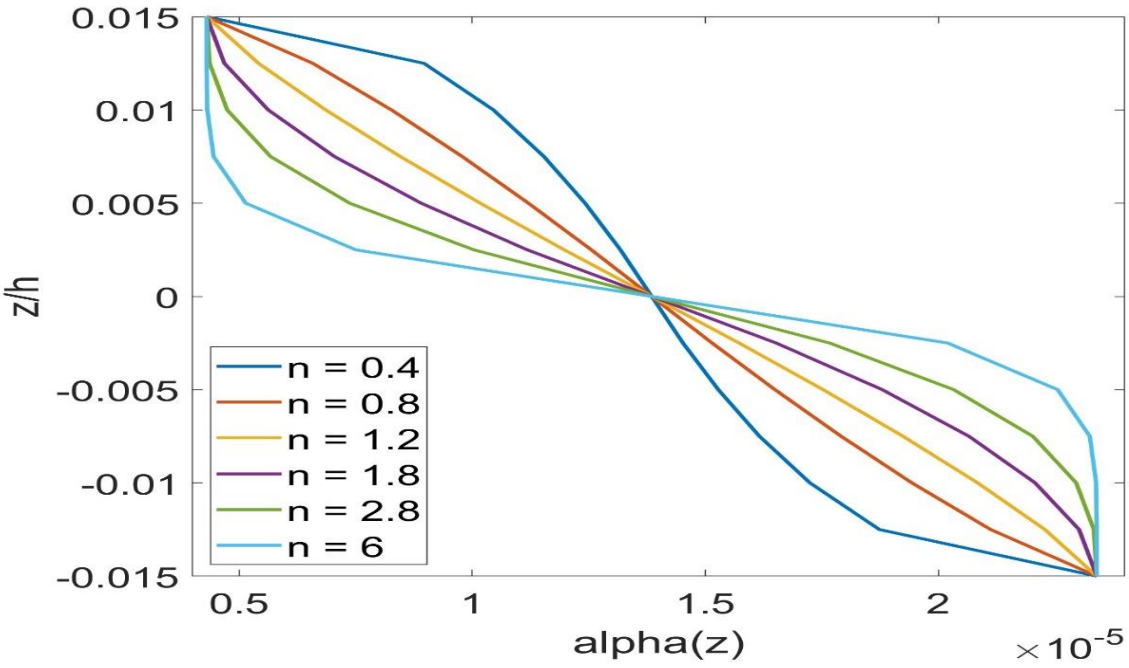

Fig 1.8: Variation of coefficient of thermal deformation with the non-dimensional thickness for different values of Sigmoid law index n.

Case 2; Mori-Tanaka technique

The results of the effective material properties of case 2 computed using the power law index distribution are presented. Table 2.1-2.4 and fig 2.1-2.1 describe the effective material properties. The following equation is used to evaluate the bulk modulus of Aluminum-ceramic FGM, shear modulus has been provided in the table 1.1, $B = \frac{E}{3(1-2\nu)}$. Calculations show that $B_1 = 58.33GPa$ and $B_2 = 215.65Gpa$.

Table 2.1: Power law Index (n) and corresponding Bulk modulus through-the-thickness.

z/h	n=0.4	0.8	1.2	1.8	2.8	6
0.0150	1.1727e+11	1.1727e+11	1.1727e+11	1.1727e+11	1.1727e+11	1.1727e+11
0.0125	1.1649e+11	1.1572e+11	1.1493e+11	1.1375e+11	1.1175e+11	1.0522e+11
0.0100	1.1564e+11	1.1399e+11	1.1232e+11	1.0978e+11	1.0550e+11	9.2126e+10
0.0075	1.1469e+11	1.1206e+11	1.0938e+11	1.0532e+11	9.8596e+10	7.9919e+10
0.0050	1.1362e+11	1.0987e+11	1.0606e+11	1.0035e+11	9.1234e+10	7.0379e+10
0.0025	1.1239e+11	1.0736e+11	1.0229e+11	9.4852e+10	8.3738e+10	6.4149e+10
0	1.1097e+11	1.0446e+11	9.7991e+10	8.8871e+10	7.6554e+10	6.0729e+10
-0.0025	1.0926e+11	1.0104e+11	9.3071e+10	8.2520e+10	7.0186e+10	5.9149e+10
-0.0050	1.0717e+11	9.6914e+10	8.7431e+10	7.6021e+10	6.5072e+10	5.8548e+10
-0.0075	1.0446e+11	9.1799e+10	8.0977e+10	6.9737e+10	6.1469e+10	5.8371e+10
-0.0100	1.0066e+11	8.5168e+10	7.3674e+10	6.4197e+10	5.9364e+10	5.8336e+10
-0.0125	9.4322e+10	7.5872e+10	6.5686e+10	6.0095e+10	5.8482e+10	5.8333e+10
-0.0150	5.8333e+10	5.8333e+10	5.8333e+10	5.8333e+10	5.8333e+10	5.8333e+10

Table 2.2: Power law Index (n) and corresponding shear modulus through-the-thickness.

z/h	n=0.4	0.8	1.2	1.8	2.8	6
0.0150	5.8301e+10	5.8301e+10	5.8301e+10	5.8301e+10	5.8301e+10	5.8301e+10
0.0125	5.8079e+10	5.7852e+10	5.7620e+10	5.7264e+10	5.6647e+10	5.4490e+10
0.0100	5.7830e+10	5.7338e+10	5.6826e+10	5.6021e+10	5.4585e+10	4.9326e+10
0.0075	5.7548e+10	5.6745e+10	5.5892e+10	5.4524e+10	5.2032e+10	4.3167e+10
0.0050	5.7225e+10	5.6050e+10	5.4780e+10	5.2711e+10	4.8927e+10	3.7058e+10
0.0025	5.6849e+10	5.5224e+10	5.3438e+10	5.0507e+10	4.5266e+10	3.2225e+10
0	5.6402e+10	5.4221e+10	5.1793e+10	4.7832e+10	4.1166e+10	2.9212e+10
-0.0025	5.5854e+10	5.2971e+10	4.9743e+10	4.4615e+10	3.6920e+10	2.7720e+10
-0.0050	5.5158e+10	5.1360e+10	4.7139e+10	4.0834e+10	3.2992e+10	2.7135e+10
-0.0075	5.4221e+10	4.9181e+10	4.3766e+10	3.6595e+10	2.9888e+10	2.6961e+10
-0.0100	5.2827e+10	4.6009e+10	3.9325e+10	3.2266e+10	2.7927e+10	2.6926e+10
-0.0125	5.0282e+10	4.0741e+10	3.3491e+10	2.8622e+10	2.7070e+10	2.6923e+10
-0.0150	2.6923e+10	2.6923e+10	2.6923e+10	2.6923e+10	2.6923e+10	2.6923e+10

Table 2.3: Power law Index (n) and corresponding Young's modulus through-the-thickness.

z/h	n=0.4	0.8	1.2	1.8	2.8	6
0.0150	1.5004e+11	1.5004e+11	1.5004e+11	1.5004e+11	1.5004e+11	1.5004e+11
0.0125	1.4941e+11	1.4876e+11	1.4811e+11	1.4711e+11	1.4538e+11	1.3941e+11
0.0100	1.4870e+11	1.4731e+11	1.4588e+11	1.4363e+11	1.3967e+11	1.2557e+11
0.0075	1.4791e+11	1.4565e+11	1.4327e+11	1.3950e+11	1.3274e+11	1.0974e+11
0.0050	1.4700e+11	1.4371e+11	1.4020e+11	1.3457e+11	1.2452e+11	9.4575e+10
0.0025	1.4594e+11	1.4142e+11	1.3654e+11	1.2868e+11	1.1506e+11	8.2809e+10
0	1.4469e+11	1.3867e+11	1.3210e+11	1.2167e+11	1.0473e+11	7.5526e+10
-0.0025	1.4317e+11	1.3527e+11	1.2666e+11	1.1341e+11	9.4235e+10	7.1925e+10
-0.0050	1.4124e+11	1.3095e+11	1.1987e+11	1.0390e+11	8.4667e+10	7.0512e+10
-0.0075	1.3867e+11	1.2519e+11	1.1126e+11	9.3440e+10	7.7159e+10	7.0091e+10
-0.0100	1.3488e+11	1.1696e+11	1.0015e+11	8.2907e+10	7.2424e+10	7.0008e+10
-0.0125	1.2809e+11	1.0367e+11	8.5879e+10	7.4101e+10	7.0356e+10	7.0000e+10
-0.0150	7.0000e+10	7.0000e+10	7.0000e+10	7.0000e+10	7.0000e+10	7.0000e+10

Table 2.4: Power law Index (n) and corresponding Poisson's ratio through-the-thickness.

z/h	n=0.4	0.8	1.2	1.8	2.8	6
0.0150	0.2868	0.2868	0.2868	0.2868	0.2868	0.2868
0.0125	0.2862	0.2857	0.2852	0.2845	0.2832	0.2792
0.0100	0.2857	0.2846	0.2835	0.2819	0.2794	0.2728
0.0075	0.2851	0.2834	0.2817	0.2793	0.2756	0.2711
0.0050	0.2844	0.2820	0.2797	0.2765	0.2725	0.2760
0.0025	0.2836	0.2805	0.2775	0.2739	0.2710	0.2849
0	0.2827	0.2788	0.2753	0.2718	0.2720	0.2927
-0.0025	0.2816	0.2769	0.2732	0.2709	0.2762	0.2973
-0.0050	0.2803	0.2748	0.2715	0.2722	0.2831	0.2993
-0.0075	0.2788	0.2727	0.2710	0.2767	0.2908	0.2999
-0.0100	0.2767	0.2711	0.2734	0.2848	0.2967	0.3000
-0.0125	0.2737	0.2723	0.2821	0.2945	0.2995	0.3000
-0.0150	0.3000	0.3000	0.3000	0.3000	0.3000	0.3000

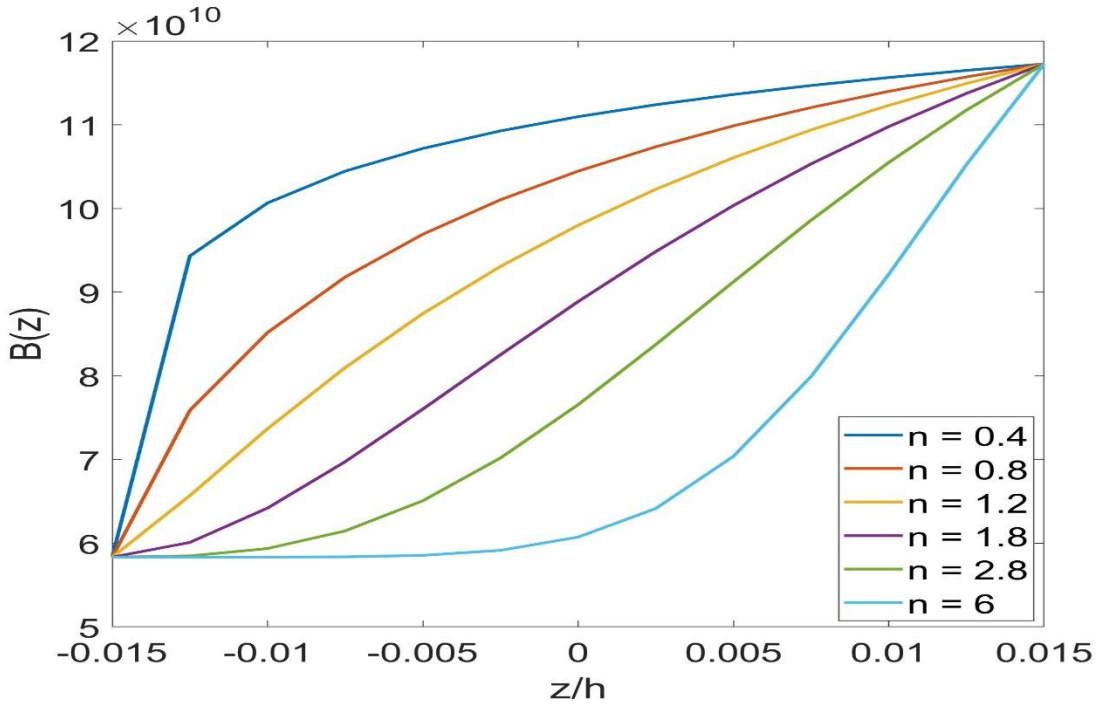

Fig 2.1: Variation of bulk modulus with the non-dimensional thickness for different values of power law index n, using Mori-Tanaka technique.

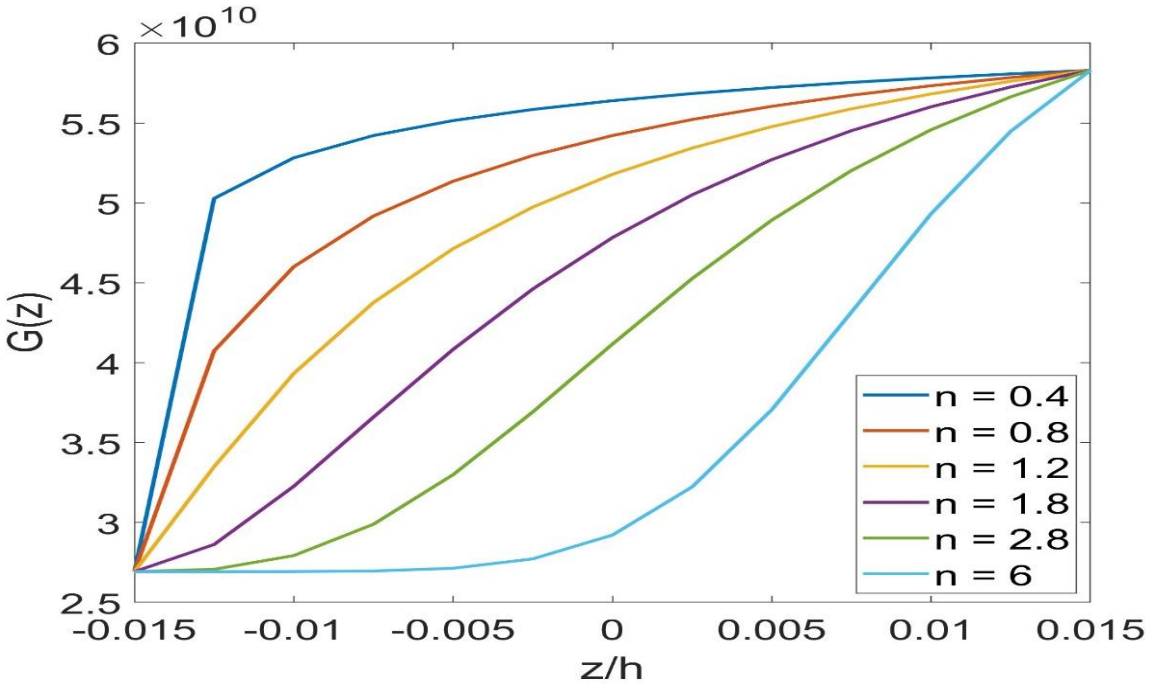

Fig 2.2: Variation of shear modulus with the non-dimensional thickness for different values of power law index n, using Mori-Tanaka technique.

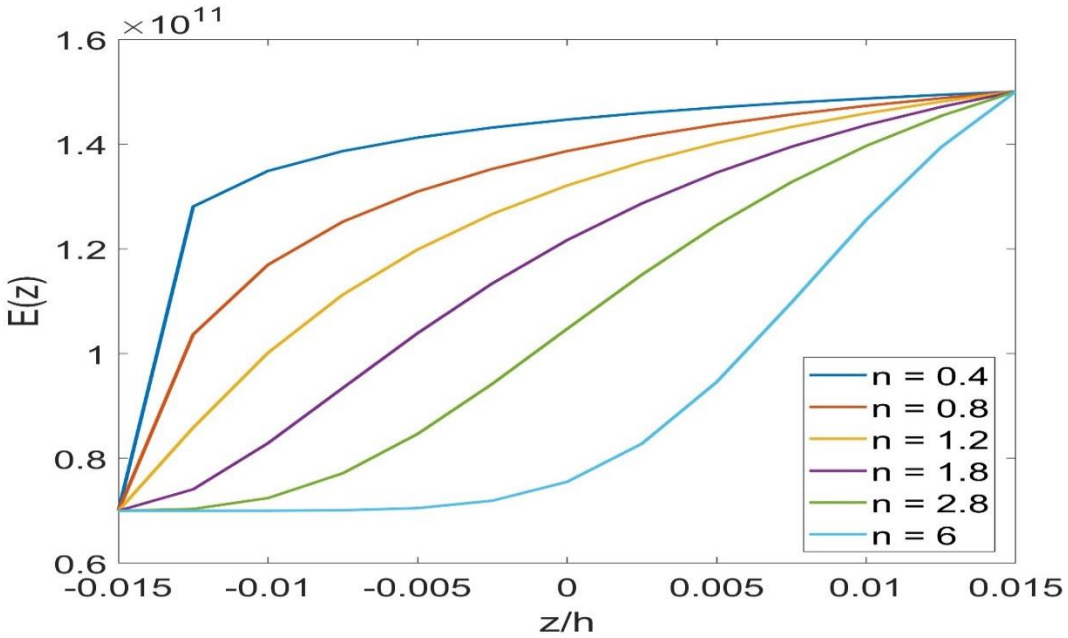

Fig 2.3: Variation of modulus of elasticity with the non-dimensional thickness for different values of power law index n, using Mori-Tanaka technique.

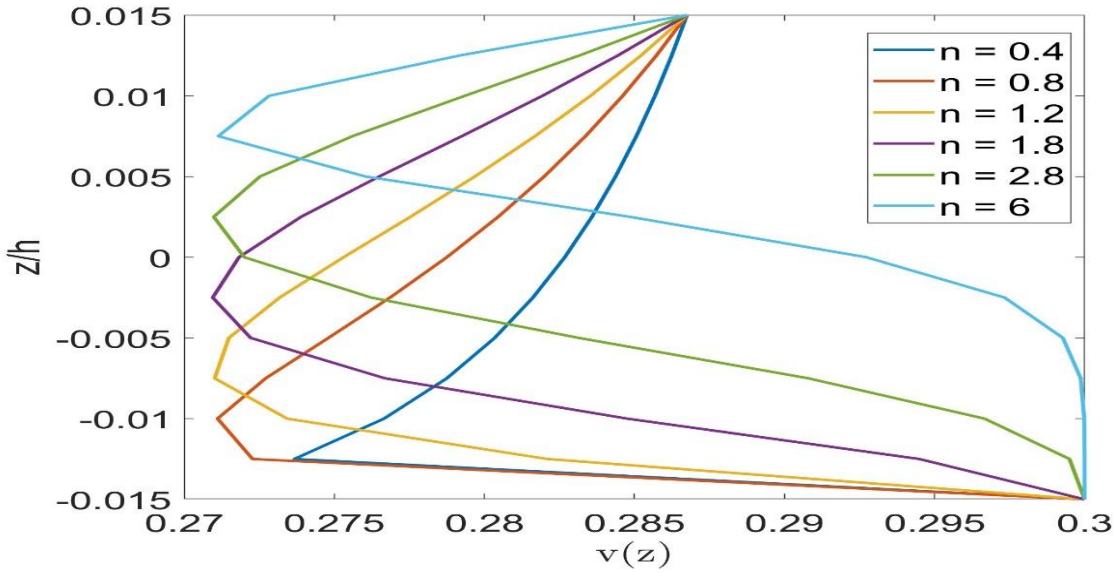

Fig 2.4: Variation of Poisson's ratio with the non-dimensional thickness for different values of power law index n, using Mori-Tanaka technique.

Result of case 2 with Sigmoid law distribution

The results of the effective material properties of case 2 computed using the sigmoid law distribution are presented. Table 2.5-2.9 and fig 2.5-2.9 describe the smooth transfer of material properties across the interface unlike the ones obtained using one single power law index.

Table 2.5: Sigmoid law index n, and corresponding Bulk modulus through-the-thickness.

z/h	n=0.4	0.8	1.2	1.8	2.8	6
0.0150	1.1727e+11	1.1727e+11	1.1727e+11	1.1727e+11	1.1727e+11	1.1727e+11
0.0125	1.1090e+11	1.1442e+11	1.1593e+11	1.1682e+11	1.1719e+11	1.1726e+11
0.0100	1.0836e+11	1.1200e+11	1.1404e+11	1.1567e+11	1.1675e+11	1.1725e+11
0.0075	1.0630e+11	1.0954e+11	1.1170e+11	1.1378e+11	1.1561e+11	1.1709e+11
0.0050	1.0448e+11	1.0695e+11	1.0887e+11	1.1100e+11	1.1332e+11	1.1627e+11
0.0025	1.0280e+11	1.0419e+11	1.0542e+11	1.0700e+11	1.0911e+11	1.1314e+11
0	1.0121e+11	1.0121e+11	1.0121e+11	1.0121e+11	1.0121e+11	1.0121e+11
-0.0025	9.9508e+10	9.7825e+10	9.6163e+10	9.3715e+10	8.9786e+10	7.8921e+10
-0.0050	9.7451e+10	9.3799e+10	9.0290e+10	8.5369e+10	7.8263e+10	6.4767e+10
-0.0075	9.4847e+10	8.8871e+10	8.3447e+10	7.6554e+10	6.8419e+10	5.9546e+10
-0.0100	9.1292e+10	8.2589e+10	7.5538e+10	6.8093e+10	6.1828e+10	5.8441e+10
-0.0125	8.5623e+10	7.3978e+10	6.6683e+10	6.1359e+10	5.8851e+10	5.8335e+10
-0.0150	5.8333e+10	5.8333e+10	5.8333e+10	5.8333e+10	5.8333e+10	5.8333e+10

Table 2.6: Sigmoid law index n, and corresponding Shear modulus through-the-thickness.

z/h	n=0.4	0.8	1.2	1.8	2.8	6
0.0150	5.8301e+10	5.8301e+10	5.8301e+10	5.8301e+10	5.8301e+10	5.8301e+10
0.0125	5.6382e+10	5.7467e+10	5.7915e+10	5.8174e+10	5.8280e+10	5.8301e+10
0.0100	5.5556e+10	5.6726e+10	5.7353e+10	5.7838e+10	5.8153e+10	5.8297e+10
0.0075	5.4863e+10	5.5943e+10	5.6634e+10	5.7275e+10	5.7819e+10	5.8252e+10
0.0050	5.4228e+10	5.5085e+10	5.5723e+10	5.6413e+10	5.7135e+10	5.8014e+10
0.0025	5.3623e+10	5.4126e+10	5.4558e+10	5.5102e+10	5.5804e+10	5.7078e+10
0	5.3034e+10	5.3034e+10	5.3034e+10	5.3034e+10	5.3034e+10	5.3034e+10
-0.0025	5.2388e+10	5.1727e+10	5.1053e+10	5.0022e+10	4.8262e+10	4.2589e+10
-0.0050	5.1577e+10	5.0058e+10	4.8496e+10	4.6111e+10	4.2201e+10	3.2741e+10

-0.0075	5.0505e+10	4.7832e+10	4.5112e+10	4.1166e+10	3.5620e+10	2.8102e+10
-0.0100	4.8953e+10	4.4652e+10	4.0530e+10	3.5374e+10	3.0211e+10	2.7029e+10
-0.0125	4.6240e+10	3.9525e+10	3.4285e+10	2.9789e+10	2.7432e+10	2.6925e+10
-0.0150	2.6923e+10	2.6923e+10	2.6923e+10	2.6923e+10	2.6923e+10	2.6923e+10

Table 2.7: Sigmoid law index n, and corresponding Young's modulus through-the-thickness.

z/h	n=0.4	0.8	1.2	1.8	2.8	6
0.0150	1.5004e+11	1.5004e+11	1.5004e+11	1.5004e+11	1.5004e+11	1.5004e+11
0.0125	1.4463e+11	1.4768e+11	1.4894e+11	1.4968e+11	1.4998e+11	1.5004e+11
0.0100	1.4234e+11	1.4560e+11	1.4736e+11	1.4872e+11	1.4962e+11	1.5003e+11
0.0075	1.4043e+11	1.4341e+11	1.4534e+11	1.4714e+11	1.4867e+11	1.4990e+11
0.0050	1.3869e+11	1.4104e+11	1.4280e+11	1.4472e+11	1.4674e+11	1.4922e+11
0.0025	1.3704e+11	1.3841e+11	1.3959e+11	1.4109e+11	1.4303e+11	1.4658e+11
0	1.3544e+11	1.3544e+11	1.3544e+11	1.3544e+11	1.3544e+11	1.3544e+11
-0.0025	1.3370e+11	1.3193e+11	1.3013e+11	1.2740e+11	1.2279e+11	1.0829e+11
-0.0050	1.3153e+11	1.2749e+11	1.2339e+11	1.1723e+11	1.0731e+11	8.4058e+10
-0.0075	1.2868e+11	1.2167e+11	1.1467e+11	1.0473e+11	9.1058e+10	7.2846e+10
-0.0100	1.2459e+11	1.1350e+11	1.0314e+11	9.0458e+10	7.7939e+10	7.0257e+10
-0.0125	1.1756e+11	1.0065e+11	8.7807e+10	7.6920e+10	7.1228e+10	7.0004e+10
-0.0150	7.0000e+10	7.0000e+10	7.0000e+10	7.0000e+10	7.0000e+10	7.0000e+10

Table 2.8: Sigmoid law index n, and corresponding Poisson's ratio through-the-thickness.

z/h	**n=0.4**	**0.8**	**1.2**	**1.8**	**2.8**	**6**
0.0150	0.2868	0.2868	0.2868	0.2868	0.2868	0.2868
0.0125	0.2826	0.2849	0.2859	0.2865	0.2867	0.2868
0.0100	0.2811	0.2833	0.2846	0.2857	0.2864	0.2867
0.0075	0.2798	0.2818	0.2831	0.2845	0.2857	0.2866
0.0050	0.2788	0.2802	0.2814	0.2827	0.2842	0.2861
0.0025	0.2778	0.2786	0.2793	0.2802	0.2815	0.2841
0	0.2769	0.2769	0.2769	0.2769	0.2769	0.2769
-0.0025	0.2761	0.2752	0.2745	0.2734	0.2721	0.2713
-0.0050	0.2751	0.2735	0.2722	0.2711	0.2715	0.2837
-0.0075	0.2739	0.2718	0.2710	0.2720	0.2782	0.2961
-0.0100	0.2725	0.2709	0.2724	0.2786	0.2899	0.2996
-0.0125	0.2712	0.2732	0.2805	0.2911	0.2983	0.3000
-0.0150	0.3000	0.3000	0.3000	0.3000	0.3000	0.3000

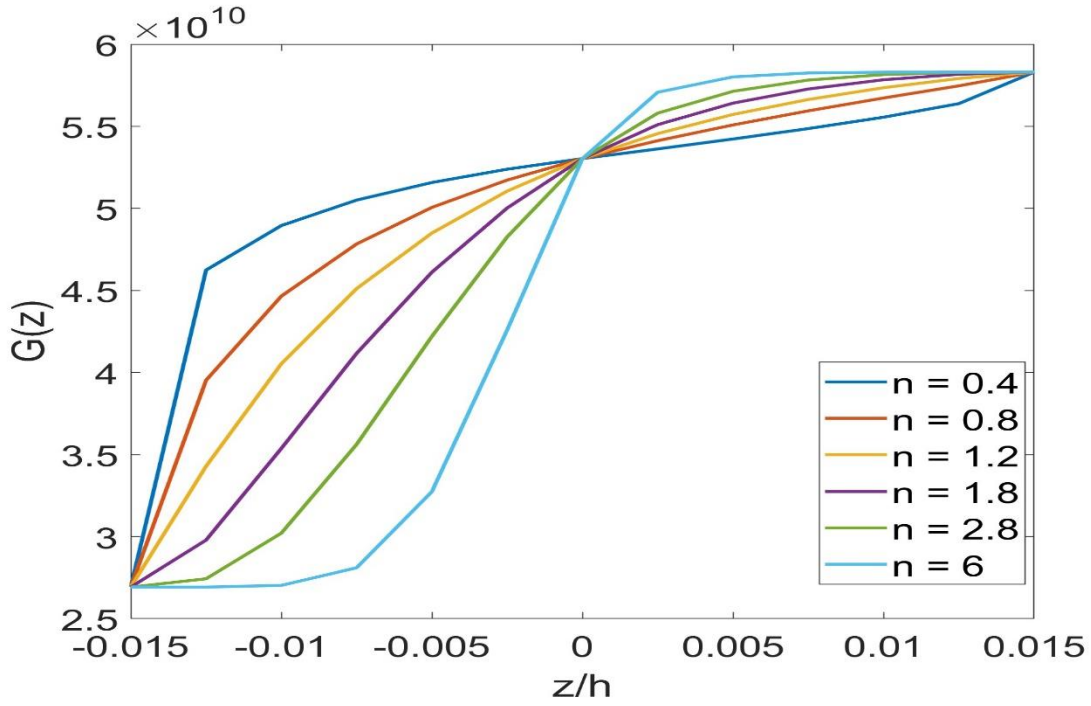

Fig 2.5: Variation of shear modulus with the non-dimensional thickness for Sigmoid law index n, using Mori-Tanaka technique.

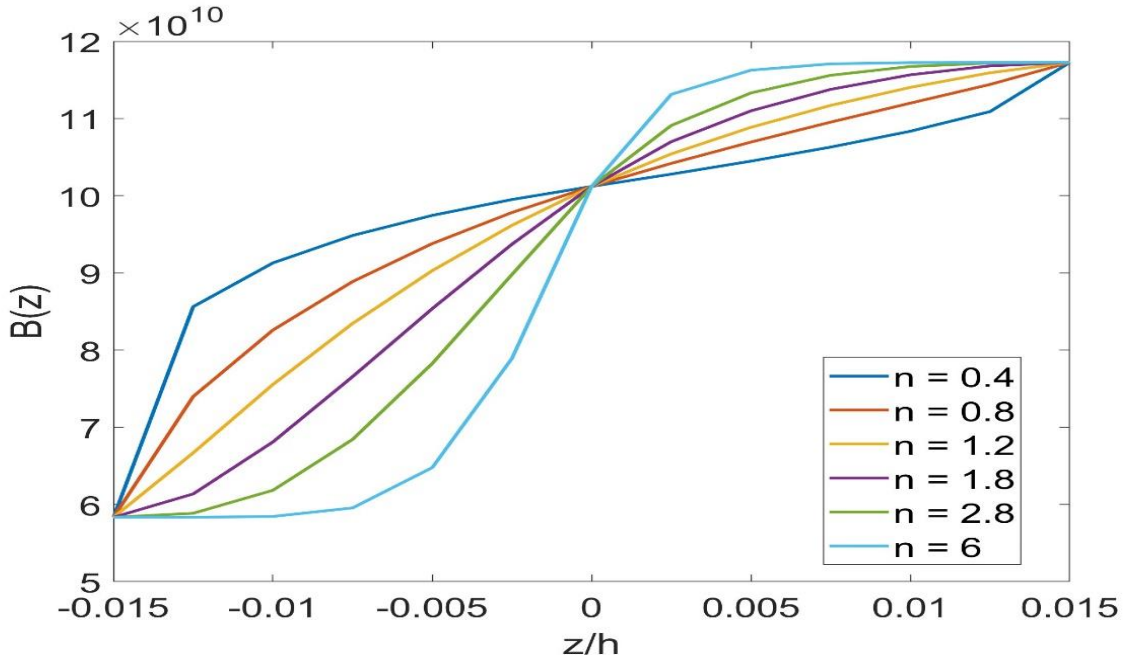

Fig 2.6: Variation of Bulk modulus with the non-dimensional thickness for Sigmoid law index n, using Mori-Tanaka technique.

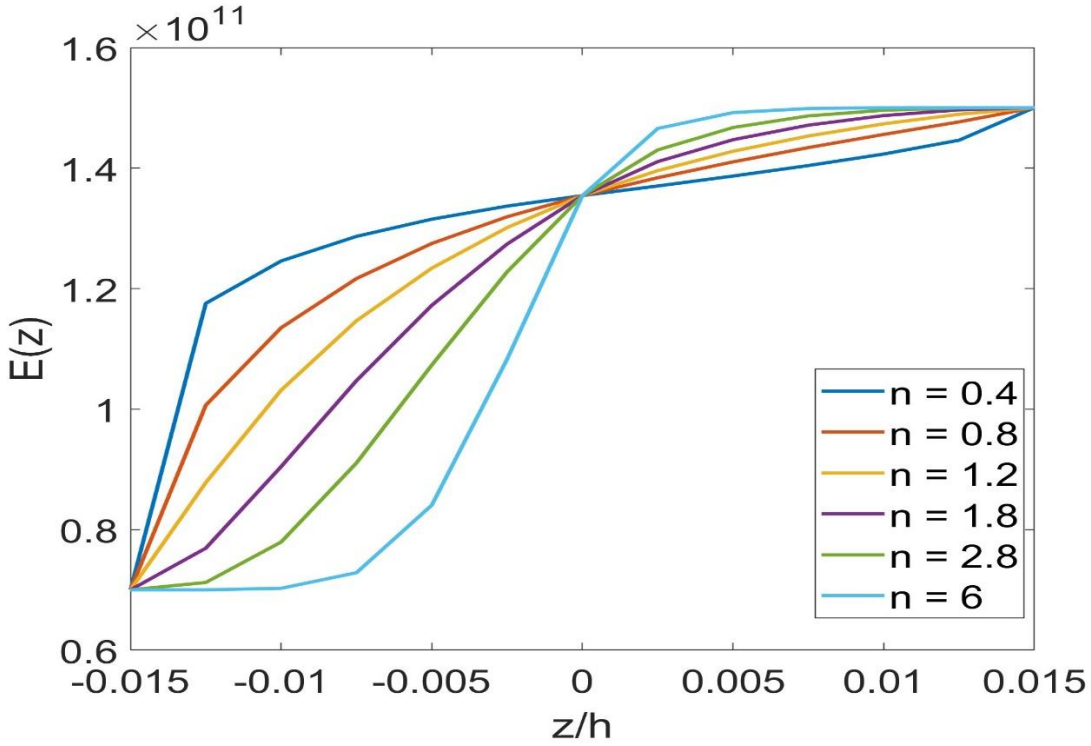

Fig 2.7: Variation of modulus of elasticity with the non-dimensional thickness for Sigmoid law index n, using Mori-Tanaka technique.

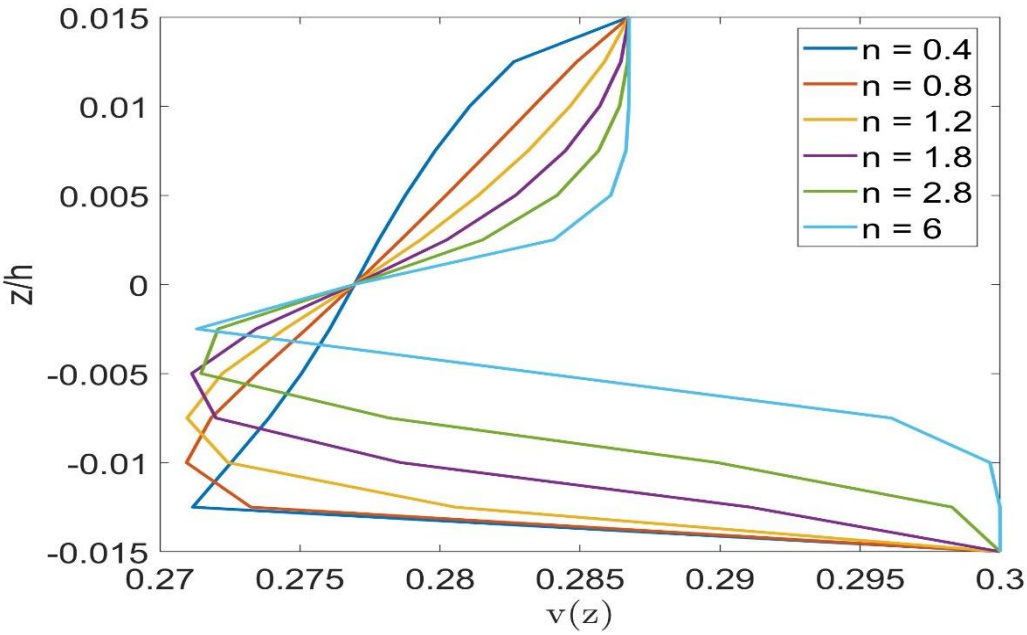

Fig 2.8: Variation of modulus of elasticity with the non-dimensional thickness for Sigmoid law index n, using Mori-Tanaka technique.

Case 3: Result of exponential law distributions

The results of the effective material properties of case 3 computed using the exponential law distribution are presented. Table 3.1 and fig 3.1 describe the exponential variation of material properties of functionaly graded material through-the-thickness.

Table3.1: Exponential law distribution of variation of material properties through-the-thickness.

z/h	$E(z)$	$V(z)$	$\alpha(z)$	$K(z)$
0.0150	4.2700e+11	0.1700	4.3000	65
0.0125	3.6727e+11	0.1782	4.9520	72.2964
0.0100	3.1589e+11	0.1869	5.7029	80.4119
0.0075	2.7170e+11	0.1959	6.5676	89.4384
0.0050	2.3370e+11	0.2054	7.5634	99.4781
0.0025	2.0101e+11	0.2154	8.7102	110.6448
0	1.7289e+11	0.2258	10.0310	123.0650
-0.0025	1.4870e+11	0.2368	11.5519	136.8794
-0.0050	1.2790e+11	0.2483	13.3035	152.2445
-0.0075	1.1001e+11	0.2603	15.3207	169.3344
-0.0100	9.4621e+10	0.2729	17.6438	188.3427
-0.0125	8.1385e+10	0.2861	20.3191	209.4847
-0.0150	7.0000e+10	0.3000	23.4000	233

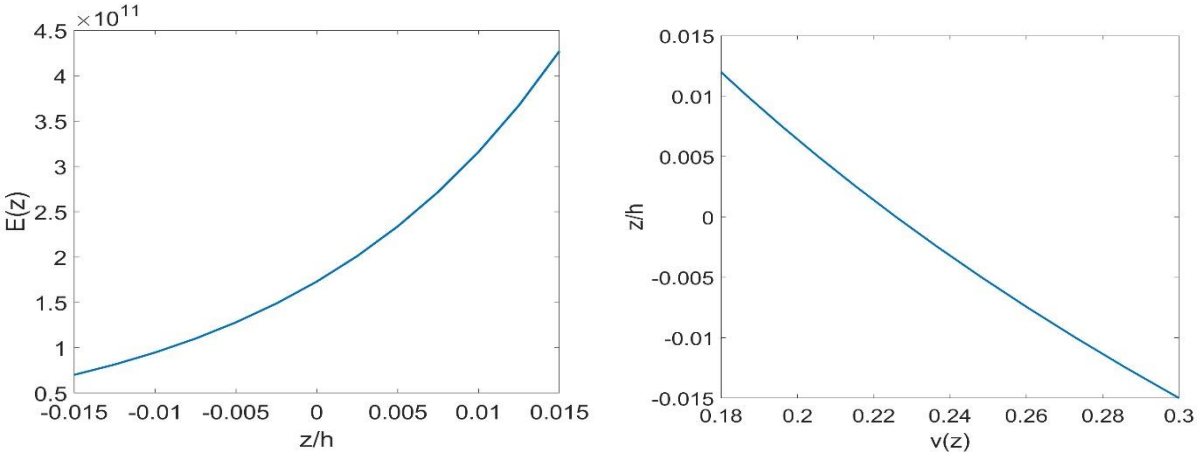

Fig3.1: Variation of Young's modulus and Poisson's ratio with the non-dimensional thickness for exponential law distributions.

Conclusion

Functionally graded materials are presented as a good replacement for composites. These materials aim to overcome the delamination problems commonly encountered in ordinary composites. They are commonly used in aerospace industrial applications where environmental factors are harsh. The analysis of effective material properties of functionally graded plates was conducted using two different homogenization schemes: the rule of mixture and the Mori–Tanaka scheme. These schemes were employed to obtain effective material properties that continuously vary through-the- thickness. It was observed that the effective material properties estimated by the rule of mixture model are larger than those obtained with the Mori–Tanaka scheme. In the single power-law function, stress concentrations appear on one of the interfaces where the material is continuous but changes rapidly across the interface. Here, the volume fraction is calculated using two power-law functions to ensure that material properties are smoothly distributed across interfaces, as described in Figures 1.6-1.9 and 2.5-2.9.

We will determine which of the two techniques provides better estimations as we study the influence of each homogenization scheme on displacements and stresses using the finite element method in our upcoming research. We will employ the equilibrium governing equations, displacement-strain relations, and relevant constitutive laws to analyze the static deformation of functionally graded composites under bi-sinusoidal loading conditions. The results obtained from each of the schemes will be compared with analytical solutions in the literature.

REFERENCES

[1] [1] F. Delale and F. Erdogan, "The crack problem for a nonhomogeneous plane," 1983.

[2] [2] M. M. Gasik, "Micromechanical modelling of functionally graded materials," Computational Materials Science, vol. 13, no. 1-3, pp. 42-55, 1998.

[3] [3] S. Srividhya, K. Basant, R. Gupta, A. Rajagopal, and J. Reddy, "Influence of the homogenization scheme on the bending response of functionally graded plates," Acta Mechanica, vol. 229, pp. 4071-4089, 2018.

[4] [4] A. Gupta and M. Talha, "Recent development in modeling and analysis of functionally graded materials and structures," Progress in Aerospace Sciences, vol. 79, pp. 1-14, 2015.

[5] [5] B. Klusemann and B. Svendsen, "Homogenization methods for multi-phase elastic composites: Comparisons and benchmarks," Technische Mechanik-European Journal of Engineering Mechanics, vol. 30, no. 4, pp. 374-386, 2010.

[6] [6] J. Reddy, "Analysis of functionally graded plates," International Journal for numerical methods in engineering, vol. 47, no. 1-3, pp. 663-684, 2000.

[7] [7] G. Praveen and J. Reddy, "Nonlinear transient thermoelastic analysis of functionally graded ceramic-metal plates," International journal of solids and structures, vol. 35, no. 33, pp. 4457-4476, 1998.

[8] [8] Z. Hashin and S. Shtrikman, "A variational approach to the theory of the elastic behaviour of multiphase materials," Journal of the Mechanics and Physics of Solids, vol. 11, no. 2, pp. 127-140, 1963.

[9] [9] Z. Hashin, "Assessment of the self consistent scheme approximation: conductivity of particulate composites," Journal of Composite Materials, vol. 2, no. 3, pp. 284-300, 1968.

[10] [10] J. R. Zuiker, "Functionally graded materials: choice of micromechanics model and limitations in property variation," Composites Engineering, vol. 5, no. 7, pp. 807-819, 1995.

[11] [11] S. S. Vel and R. Batra, "Exact solution for thermoelastic deformations of functionally graded thick rectangular plates," AIAA journal, vol. 40, no. 7, pp. 1421-1433, 2002.

[12] [12] T. Mori and K. Tanaka, "Average stress in matrix and average elastic energy of materials with misfitting inclusions," Acta metallurgica, vol. 21, no. 5, pp. 571-574, 1973.

[13] [13] F. Moleiro, V. F. Correia, A. Araújo, C. M. Soares, A. Ferreira, and J. Reddy, "Deformations and stresses of multilayered plates with embedded functionally graded material layers using a layerwise mixed model," Composites part B: engineering, vol. 156, pp. 274-291, 2019.

[14] [14] Y. Benveniste, "A new approach to the application of Mori-Tanaka's theory in composite materials," Mechanics of materials, vol. 6, no. 2, pp. 147-157, 1987.

[15] [15] J. R. Willis, "Bounds and self-consistent estimates for the overall properties of anisotropic composites," Journal of the Mechanics and Physics of Solids, vol. 25, no. 3, pp. 185-202, 1977.

[16] [16] R. Hill, "A self-consistent mechanics of composite materials," Journal of the Mechanics and Physics of Solids, vol. 13, no. 4, pp. 213-222, 1965.

[17] [17] K. Bhaskar and T. Varadan, "The contradicting assumptions of zero transverse normal stress and strain in the thin plate theory: A justification," 2001.

[18] [18] H.-S. Shen and Z.-X. Wang, "Assessment of Voigt and Mori–Tanaka models for vibration analysis of functionally graded plates," Composite Structures, vol. 94, no. 7, pp. 2197-2208, 2012.

[19] [19] A. J. M. Ferreira, C. M. C. Roque, R. M. N. Jorge, G. E. Fasshauer, and R. C. Batra, "Analysis of Functionally Graded Plates by a Robust Meshless Method," Mechanics of Advanced Materials and Structures, vol. 14, no. 8, pp. 577-587, 2007, doi: 10.1080/15376490701672732.

[20] [20] A. J. M. Ferreira, R. C. Batra, C. M. C. Roque, L. F. Qian, and P. A. L. S. Martins, "Static analysis of functionally graded plates using third-order shear deformation theory and a meshless method," Composite Structures, vol. 69, no. 4, pp. 449-457, 2005, doi: 10.1016/j.compstruct.2004.08.003.

[21] [21] J. Reddy and Z.-Q. Cheng, "Three-dimensional thermomechanical deformations of functionally graded rectangular plates," European Journal of Mechanics-A/Solids, vol. 20, no. 5, pp. 841-855, 2001.

[22] [22] M. Bhandari and K. Purohit, "Response of functionally graded material plate under thermomechanical load subjected to various boundary conditions," International Journal of Metals, vol. 2015, 2015.

[23] [23] Z.-Q. Cheng and R. Batra, "Three-dimensional thermoelastic deformations of a functionally graded elliptic plate," Composites Part B: Engineering, vol. 31, no. 2, pp. 97-106, 2000.

[24] [24] M. S. Medeiros Jr, E. Parente Jr, and A. M. C. d. Melo, "Influence of the Micromechanics Models and Volume Fraction Distribution on the Overall Behavior of SiC/Al Functionally Graded Pressurized Cylinders," Latin American Journal of Solids and Structures, vol. 16, no. 4, 2019, doi: 10.1590/1679-78255433.

[25] [25] D. Jha, T. Kant, and R. Singh, "A critical review of recent research on functionally graded plates," Composite structures, vol. 96, pp. 833-849, 2013.

[26] [26] F. Moleiro, E. Carrera, A. J. M. Ferreira, and J. N. Reddy, "Hygro-thermo-mechanical modelling and analysis of multilayered plates with embedded functionally graded material layers," Composite Structures, vol. 233, 2020, doi: 10.1016/j.compstruct.2019.111442.

AUTHORS

First Author – Christian Mathew, Department of Engineering Mechanics, Virginia Polytechnic Institute and State University, Blacksburg, 24061

Second Author – Oluomachi Ejiofor, Department of Computer Science, Austin Peay State University, Clarksville, Tennessee, 37044